

The N_{eff} at CMB challenges $U(1)_X$ light gauge boson scenarios

Dilip Kumar Ghosh,^{1,*} Purusottam Ghosh,^{2,†} Sk Jeessun,^{1,‡} and Rahul Srivastava^{3,§}

¹*Indian Association for Cultivation of Science,*

2A & 2B Raja S C Mullick Road, Kolkata 700032, India

²*Institute of Physics, Sachivalaya Marg, Bhubaneswar, 751 005, India ; Homi Bhabha National Institute, Training School Complex, Anushakti Nagar, Mumbai 400 094, India*

³*Department of Physics, Indian Institute of Science Education and Research - Bhopal Bhopal Bypass Road, Bhauri, Bhopal, India*

Abstract

The relativistic degrees of freedom (N_{eff}) is one of the crucial cosmological parameters. The precise measurement of N_{eff} at the time of cosmic microwave background formation, by Planck 2018 can be used to understand the new fundamental interactions, in particular involving light mediators. Presence of any new particle with sufficient energy density and sizeable interactions with Standard Model particles at the temperature around $\sim \text{MeV}$ can significantly alter the neutrino decoupling and hence N_{eff} . Thus the bound on N_{eff} can place stringent constraints on various beyond Standard Model paradigms involving light particles. $U(1)_X$ models are among such scenarios and are widely studied in several aspects. In this work, we consider several popular $U(1)_X$ models with light Z' boson like $U(1)_{B-L}$, $U(1)_{B-3L_i}$, $U(1)_{B_i-3L_j}$, $U(1)_{L_i-L_j}$; $i, j = 1, 2, 3$ being the flavour indices and study their impact on N_{eff} . We also examine the constraints from ground based experiments like Xenon1T, Borexino, trident, etc. Our analysis shows that for light mass $M_{Z'} \lesssim \mathcal{O}(\text{MeV})$ the N_{eff} provides the most stringent constraints on the Z' mass and coupling, far exceeding the existing constraints from other experiments.

1. INTRODUCTION

The Cosmic Microwave Background (CMB) radiations play a crucial role in elucidating the dynamics of the early universe as well as shaping our present understanding of the large-scale structure of the universe. Observations of the CMB, including temperature

*Electronic address: dilipghoshjal@gmail.com

†Electronic address: pghoshiitg@gmail.com

‡Electronic address: skjeesun48@gmail.com

§Electronic address: rahul@iiserb.ac.in

anisotropies, polarization patterns, matter-energy distribution, reionization phenomena in the early universe, are consistent with both the standard Λ CDM cosmology and the Standard Model of particle physics (SM) [1]. One of the interesting cosmological parameters N_{eff} , which represents the number of relativistic degrees of freedom at the CMB scale ($T \sim \text{eV}$), serves an important role in understanding the dynamics of the thermal history during the epoch $T \sim \text{MeV}$ to eV . At high temperature of the universe, photons and neutrinos shared the same temperature. As the universe cooled down ($T \lesssim 2 \text{ MeV}$) and the interaction rate fell below the Hubble expansion rate (H), neutrinos decoupled from photons, resulting in the formation of two separate baths i.e. neutrino bath and photon bath (combined with electrons). At temperature $T \lesssim m_e$, the two baths evolve with different temperature [1]. The parameter N_{eff} is then parameterized by the ratio of energy densities in the neutrino and photon baths. In the particle content of the SM, one can expect the neutrino decoupling event to take place around $T \sim 2 \text{ MeV}$, resulting in $N_{\text{eff}}^{\text{SM}} = 3.046$ at the CMB [2, 3]. Note the slight deviation in N_{eff} from the expected three light neutrino degrees of freedom in SM ($3 \nu_L$) is due to non-instantaneous neutrino decoupling, finite temperature QED corrections, and neutrino flavor oscillations [2, 3]. Observations of the CMB by the Planck

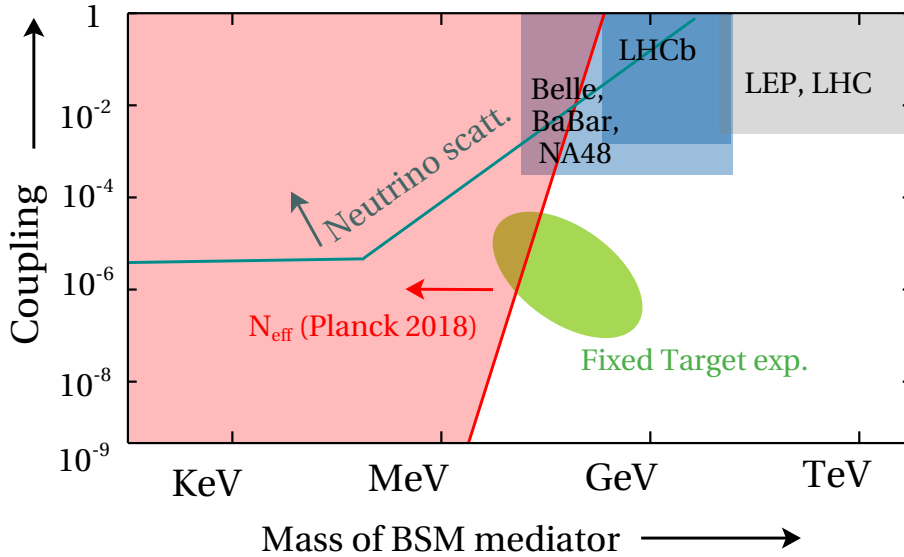


FIG. 1: Schematic diagram of the constraint from N_{eff} along with existing constraints for light mediator models. This schematic diagram assumes universal coupling of the mediator to both quarks and the leptons. Note that additional bounds may apply as well as some of these bounds can be relaxed depending on the specific details of different models.

satellite can also measure the parameter N_{eff} ¹. The latest Planck 2018 data provides a

¹ Measurements of baryon acoustic oscillations (BAO), large-scale structure (LSS) datasets, and other cosmological probes contribute to determining the value of N_{eff} [4, 5].

precise measurement of N_{eff} at the time of the CMB to be $2.99^{+0.34}_{-0.33}$ with 95% confidence level (CL), under the assumption of standard Λ CDM cosmology [5]. The upper limit of the Planck data suggests an additional contribution (apart from SM) to N_{eff} , extending up to 0.28 ($\Delta N_{\text{eff}} = N_{\text{eff}}^{\text{obs}} - N_{\text{eff}}^{\text{SM}}$), providing the hint for BSM physics.

The presence of beyond standard model (BSM) light mediators, interacting with either the photon or neutrino bath at temperatures relevant to neutrino decoupling, introduces additional contributions to the radiation energy density, leading to an increase in N_{eff} [6–8]². The observations of N_{eff} impose constraints on the BSM light mediators, as presented by the red shaded region in the cartoon Fig. 1. In certain mass regions of these mediators, N_{eff} turns out to be a severe constraint compared to other existing bounds. $U(1)_X$ models are among such widely studied BSM paradigms with light mediators and their phenomenological consequences have been explored in several contexts³. In this work, we consider light gauge boson (Z') originating from different types of $U(1)_X$ gauge extended scenarios, which naturally involve interactions with neutrinos and electron-positron pairs (either at the tree level or loop-induced). The BSM interactions in the presence of light Z' can potentially modify the late-time dynamics between the photon and neutrino baths, prolonging the process of neutrino decoupling and increasing the N_{eff} value. As a result, the upper limit on N_{eff} (3.33 with 95% CL) derived from the CMB can be utilized to constrain both the mass of the light gauge boson ($M_{Z'}$) and its corresponding gauge coupling (g_X).

In the context of N_{eff} , various types of gauged $U(1)_X$ scenarios have been explored in the existing literature. These scenarios aim to explain the excess of N_{eff} observed in the CMB, involving $U(1)_{L_\mu-L_\tau}$ [7], $U(1)_{B-L}$ [8] or, generic $U(1)_X$ model [23]. A comprehensive discussion on N_{eff} within the generic $U(1)_X$ scenario is presented in Ref. [23], categorizing $U(1)_X$ models into two classes: (i) those with tree-level coupling of Z' with electron and (ii) those without tree-level coupling of Z' with electron. The study also highlights that the varying $U(1)_X$ charges for $e, \nu_{e,\mu,\tau}$, corresponding to various gauged extended scenarios, notably impact the value of N_{eff} . This work is an extension of Ref. [23], where we consider a variety of $U(1)_X$ models, such as $U(1)_{B-L}$, $U(1)_{L_i-L_j}$ ($i \neq j$), $U(1)_{B-3L_i}$, and $U(1)_{B_i-L_j}$ etc., and study their impact on N_{eff} , assuming the scenario where Z' was initially ($T > M_{Z'}$) in thermal bath (which requires $g_X \gtrsim \mathcal{O}(10^{-9})$). The primary objective of this work is to identify the exclusion regions in the $M_{Z'} - g_X$ plane for each gauged extended model, guided by the upper bound on N_{eff} derived from CMB observations [5].

The gauged extended models are also motivated by their potential detectability across a broad mass range, from eV to TeV, as sketched in Fig. 1. For gauge boson Z' with TeV or sub TeV masses, the most severe constraints are derived from collider experiments like LHC [24–27] and LEP [28]. Whereas, in the mass range spanning from a few MeV to a few GeV,

² Note additional contributions to N_{eff} may also come from various other sources like extra radiation [9–12], models involving early dark energy [10, 13], and relativistic decaying dark matter [14].

³ See for example Ref. [15–22] and the references therein.

experiments carried out by LHCb [29], Belle[30], BaBar [31], and fixed target experiments [16, 32] are notably more effective in providing constraints. In the sub GeV mass region, with $g_X \gtrsim \mathcal{O}(10^{-6})$, the low energy neutrino scattering experiments (neutrino electron scattering [18], neutrino-nucleus scattering [33] etc.), provide most stringent constraints. However, in the mass range where $M_{Z'} \lesssim \mathcal{O}(\text{MeV})$ and $g_X \lesssim \mathcal{O}(10^{-6})$, direct searches become less sensitive. Furthermore, as we will show, CMB observations in terms of N_{eff} play a significant role in constraining the parameter space for $M_{Z'} \lesssim \mathcal{O}(\text{MeV})$. In this work, we identify the CMB exclusion region with 95% CL for each $U(1)_X$ scenario and compare it to the other aforementioned existing constraints in the $M_{Z'} - g_X$ plane. We highlight that in certain regions of $M_{Z'}$ and coupling g_X , observations of N_{eff} in the CMB provide more stringent constraints compared to other observations. We present a schematic diagram in Fig.1, where various existing constraints are summarised by different color patches based on the mass and coupling. Our key focus in this study is the red-shaded region, which represents the exclusion region derived from N_{eff} observations in the CMB.

The paper is organized in the following way. In section 2, we provide a brief overview of the evolution of N_{eff} in the presence of a light Z' , with a focus on its dependence on the gauge extension. Then we present the exclusion regions in the $M_{Z'} - g_X$ plane for various $U(1)_X$ models, determined by the upper bound on N_{eff} derived from CMB observations in section 3. Finally, in section 4 we summarize our results and conclusions.

2. EVALUATION OF N_{eff} IN LIGHT Z' MODELS

Before going to the N_{eff} analysis of light Z' emerging from various $U(1)_X$ symmetries we present a brief and generic overview of the effective Z' models in this section. The discussion in this section is based on our previous work [23] where we have presented a comprehensive analysis of N_{eff} for a generic $U(1)_X$ model. For a generic $U(1)_X$ model, we assume that SM quark doublets (Q_i) and singlets (u_i, d_i), as well as lepton doublets (L_i) and singlets (ℓ_i) are charged under this $U(1)_X$ symmetry⁴. We also need a SM singlet scalar σ carrying $U(1)_X$ charge to generate the mass of Z' ($M_{Z'}$) by acquiring a vacuum expectation value (VEV) to break the $U(1)_X$ symmetry. As pointed out in Ref. [23] that to affect the ν_L decoupling Z' has to be in the MeV scale. To keep $M_{Z'}$ very light compared to the SM Z gauge boson ($M_{Z'}^2 \ll M_Z^2$), we consider $U(1)_X$ charge of the SM Higgs doublet $\mathbb{X}_\Phi = 0$ and hence $M_{Z'}^2$ does not get any contribution from the SM vev. The charge assignments are shown in Table I.

Note that to generate the SM quark and charged lepton masses, we take the following $U(1)_X$ charge assignments: $\mathbb{X}_{Q_i} = \mathbb{X}_{u_i} = \mathbb{X}_{d_i}$ and $\mathbb{X}_{L_i} = \mathbb{X}_{\ell_i}$. It is also worth highlighting that

⁴ Note that for now we have left the $U(1)_X$ charges of SM particles as free parameters, whose values depend on the details of the $U(1)_X$ symmetry, see Table I.

although the $U(1)_X$ charges of quark doublet should be the same as that of the up and down quark singlets, the charges may differ across different generations i.e. $\mathbb{X}_{Q_1} \neq \mathbb{X}_{Q_2} \neq \mathbb{X}_{Q_3}$ as shown in Table I.

Besides the particle mentioned in Table I, we also need right-handed neutrino (RHN) ν_R for anomaly cancellation and light neutrino mass generation [15, 23, 34, 35]. In this work, we consider only Majorana type mass models where, ν_R are also too heavy to affect ν_L decoupling [36, 37] and we ignore their contribution⁵. Apart from the minimal particle content of Table I, most of the popular $U(1)_X$ models studied in literature may also contain additional BSM particles which are typically much heavier than MeV scale and will not take part in our analysis [15].

Models	$\mathbb{X}_{Q_i}(\mathbb{X}_{u_i} = \mathbb{X}_{d_i})$	\mathbb{X}_{L_1}	\mathbb{X}_{L_2}	\mathbb{X}_{L_3}
B – L	(1/3, 1/3, 1/3)	−1	−1	−1
B – 3L_e	(1/3, 1/3, 1/3)	−3	0	0
$B - 3L_\mu$	(1/3, 1/3, 1/3)	0	−3	0
$B - 3L_\tau$	(1/3, 1/3, 1/3)	0	0	−3
L_e – L_μ	(0, 0, 0)	1	−1	0
L_e – L_τ	(0, 0, 0)	1	0	−1
$L_\mu - L_\tau$	(0, 0, 0)	0	1	−1
B₁ – 3L_e	(1, 0, 0)	−3	0	0
B₂ – 3L_e	(0, 1, 0)	−3	0	0
B₃ – 3L_e	(0, 1, 0)	−3	0	0
$B_1 - 3L_\mu$	(1, 0, 0)	0	−3	0
$B_2 - 3L_\mu$	(0, 1, 0)	0	−3	0
$B_3 - 3L_\mu$	(0, 1, 0)	0	−3	0
$B_1 - 3L_\tau$	(1, 0, 0)	0	0	−3
$B_2 - 3L_\tau$	(0, 1, 0)	0	0	−3
$B_3 - 3L_\tau$	(0, 1, 0)	0	0	−3

TABLE I: $U(1)_X$ gauge charge assignments of SM particles for different models. To ease our notation throughout this paper we denote $\mathbb{X}_{L_i} = \mathbb{X}_{\ell_i}$. The models with tree level $Z'e^+e^-$ vertex ($\mathbb{X}_1 \neq 0$) are written in bold front. The charges of ν_{R_i} are fixed by anomaly cancellation condition and the charge of the scalar singlet σ , needs to give mass to Z' , depending on the model and details of neutrino mass generation.

⁵ In Dirac-type mass models, ν_R are relativistic at MeV temperature and can significantly alter N_{eff} [9].

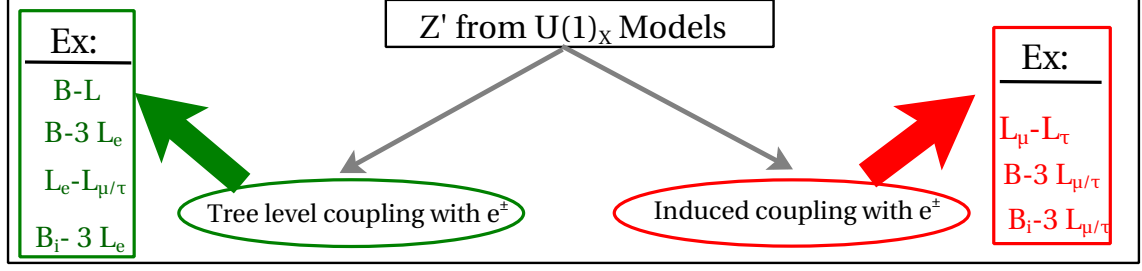


FIG. 2: The $U(1)_X$ models can be broadly classified into two categories: (a) those where Z' couples at tree level with electrons ($\mathbb{X}_1 \neq 0$), encircled in green color and (b) those where Z' has no tree level coupling with electrons ($\mathbb{X}_1 = 0$), encircled in red color. See text for more details.

The ν_L decoupling is governed by only the weak interaction processes in SM scenario and usually takes place at around $T \sim \text{MeV}$ temperature [6]. The only particles relevant at that temperature are e^\pm , γ and ν_i ($i \equiv e, \mu, \tau$). The scenario changes drastically in the presence of any light (mass $\sim \mathcal{O}(1)$ MeV) BSM particles interacting with either of these three sectors [7, 23]. Thus one can easily anticipate that light $U(1)_X$ gauge boson Z' (with mass, $M_{Z'} \sim \mathcal{O}(1)$ MeV) interacting with ν_i and e^\pm will significantly alter the N_{eff} at the time of CMB. In this work we will assume all 3 ν_i acquire the same temperature (T_{ν_L}) and consider the case where Z' was initially in a thermal bath ($g_X \gtrsim 10^{-9}$) [23]. N_{eff} is parametrised in terms of the temperature ratios of ν_i sector and γ bath [1],

$$N_{\text{eff}} = \frac{8}{7} \left(\frac{11}{4} \right)^{4/3} \left(\frac{\rho_{\nu_L}(T_{\nu_L})}{\rho_\gamma(T_\gamma)} \right) = 3 \times \frac{8}{7} \left(\frac{11}{4} \right)^{4/3} \left(\frac{T_{\nu_L}}{T_\gamma} \right)^4 \quad (1)$$

N_{eff} at the time of CMB is determined by computing the temperature ratio $\frac{T_{\nu_L}}{T_\gamma}$ at $T_\gamma = T_{\text{CMB}}$. Note that, throughout this paper, whenever we say N_{eff} , we refer N_{eff} at the time of CMB. To evaluate T_{ν_L}/T_γ we solve the following coupled equations ⁶,

$$\frac{dT_{\nu_L}}{dt} = - \left(4H\rho_{\nu_L} - \frac{\delta\rho_{\nu_L \rightarrow e^\pm}}{\delta t} + \frac{\delta\rho_{Z' \rightarrow \nu_L}}{\delta t} \right) \left(\frac{\partial\rho_{\nu_L}}{\partial T_{\nu_L}} \right)^{-1} \quad (2)$$

$$\frac{dT_{Z'}}{dt} = - \left(3H(\rho_{Z'} + P_{Z'}) - \frac{\delta\rho_{Z' \rightarrow \nu_L}}{\delta t} - \frac{\delta\rho_{Z' \rightarrow e^\pm}}{\delta t} \right) \left(\frac{\partial\rho_{Z'}}{\partial T_{Z'}} \right)^{-1} \quad (3)$$

$$\frac{dT_\gamma}{dt} = - \left(4H\rho_\gamma + 3H(\rho_e + P_e) + \frac{\delta\rho_{\nu_L \rightarrow e^\pm}}{\delta t} + \frac{\delta\rho_{Z' \rightarrow e^\pm}}{\delta t} \right) \left(\frac{\partial\rho_\gamma}{\partial T_\gamma} + \frac{\partial\rho_e}{\partial T_\gamma} \right)^{-1}, \quad (4)$$

where, ρ_r, P_r and T_r stand for the energy density, pressure density, and temperature of species r . On the other hand, $\frac{\delta\rho_{a \rightarrow b}}{\delta t}$ signify the energy transfer rate from bath a to b , deduced by integrating the collision terms [7, 23]. As mentioned earlier, assuming same

⁶ Further details can be found in Appendix A-C of Ref. [23].

temperature between 3 ν_i sectors, we denote $\rho_{\nu_L} = \sum_{i=e,\mu,\tau} \rho_{\nu_i}$, $\frac{\delta\rho_{\nu_L \rightarrow e}}{\delta t} = \sum_{i=e,\mu,\tau} \frac{\delta\rho_{\nu_i \rightarrow e}}{\delta t}$ and $\frac{\delta\rho_{Z' \rightarrow \nu_L}}{\delta t} = \sum_{i=e,\mu,\tau} \frac{\delta\rho_{Z' \rightarrow \nu_i}}{\delta t}$. Throughout the paper, by ν_L we refer all 3 generation of ν_i ($i \equiv e, \mu, \tau$) as a whole. We do not discuss the energy transfer rates here as they are already elaborated in detail in Ref. [23].

It is worth mentioning that the $\nu_i \bar{\nu}_i Z'$ coupling and the $e^+ e^- Z'$ coupling are the most crucial parameters in the BSM processes that affect the N_{eff} . However, interactions involving heavier charged leptons and quarks are insignificant here, as their energy densities are suppressed at temperatures nearing ~ 1 MeV. When Z' has coupling to both ν_L and e^\pm ($\mathbb{X}_1 \neq 0$), both the following BSM processes affect ν_L decoupling: (i) Z' decaying to both $e^+ e^-$ and $\nu_i \bar{\nu}_i$ and (ii) scattering process $\nu_i \bar{\nu}_i \rightarrow e^+ e^-$ mediated by Z' . Any increase in the effective coupling ($\mathbb{X}_1 g_X$) dictating these BSM processes enhances the BSM contribution, thus leading to an increment in N_{eff} . On the other hand in the absence of tree level $Z' e^+ e^-$ vertex ($\mathbb{X}_1 = 0$), all the number density of Z' finally gets diluted to ν_L bath (with 100% branching ratio) irrespective of the coupling strength ($\mathbb{X}_{2/3} g_X$). Hence for such models ($\mathbb{X}_1 = 0$), the final N_{eff} becomes independent of effective couplings $\mathbb{X}_{2,3} g_X$. Thus following our argument in Ref. [23] the light Z' models can be broadly classified into two cases: $\mathbb{X}_1 \neq 0$ and $\mathbb{X}_1 = 0$, depending on whether Z' has tree level coupling with electron or not (see Fig. 2).

It is worth highlighting that even in the absence of tree level $Z' e^+ e^-$ interaction ($\mathbb{X}_1 = 0$), induced coupling with e^\pm may exist which varies depending on the specific model [38]. We do not delve into the details of induced coupling which may arise from kinetic mixing or can be loop induced. We take the following effective $Z' e^+ e^-$ interaction Lagrangian:

$$\mathcal{L}_{\text{int}} = (\epsilon e) \bar{e} \gamma^\mu e Z'_\mu, \quad (5)$$

with a benchmark value $\epsilon = -\frac{g_X}{70}$, which is very commonly used for $L_\mu - L_\tau$ models (with $\mathbb{X}_1 = 0$) [7, 39]. Needless to say that with the increase in $M_{Z'}$, the energy density of Z' gets suppressed and hence N_{eff} decreases for both of the above mentioned two cases.

The excess in N_{eff} at CMB in the presence of Z' can be used to constrain the parameter space, as the deviation from SM predicted value of N_{eff} is also very precisely constrained from Planck 2018 [5]. We translate this constrain from N_{eff} in the parameter space of $M_{Z'} - g_X$ plane for previously mentioned two classes of generic $U(1)_X$ models in our previous work [23]. We extend this exercise for all popular $U(1)_X$ models by performing exhaustive numerical scans on the parameter space (for N_{eff}), in the next section.

3. SPECIFIC $U(1)_X$ SYMMETRIES

In this section, we will discuss some phenomenological consequences of various well motivated $U(1)_X$ symmetries. As mentioned earlier, while doing this we consider that the corresponding gauge boson Z' was initially in thermal equilibrium and the RHNs are heavy

enough that they do not take part in ν_L decoupling. In order to estimate N_{eff} , we find the temperature ratio T_{ν_L}/T_γ at $T_\gamma = T_{\text{CMB}}$ by solving eq.(2)-(4) and then plug into eq.(1). As described earlier the value of N_{eff} is strongly dependent on parameters: g_X and $M_{Z'}$, and hence the upper limit on N_{eff} by Planck 2018 [5] leads to strong constraint on the same parameter space. Before going into the details of the results we summarize the existing laboratory-based constraints on light Z' in Table-II. The detailed discussion on existing constraints can be found in Ref. [16–21]. In addition to the constraints mentioned in the table, the light Z' may also encounter astrophysical constraints like SN1987A [40–42]. However, this supernova constraint differs depending on the specific gauge model and requires a detailed analysis which is beyond the scope of this work.

Experiments	Process	Observations	Refs.
$\text{E}\nu\text{ES}$ (elastic electron-neutrino scattering)	$\nu e \rightarrow \nu e$ incoming particle: solar ν (ν_e)	recoil rate of e^-	XENON [20, 43], LZ[21], Borexino [18, 19, 44]
$\text{CE}\nu\text{NS}$ (coherent elastic neutrino -nucleus scattering)	$\nu N \rightarrow \nu N$ nuclei N: {CsI, Ar}	recoil rate of nucleus	CsI and Ar [33, 39, 45] XENON [20, 21]
Fixed target experiments	$e(p) N \rightarrow e(p) N Z'$ $Z' \rightarrow e^+e^-$	displaced vertex with di-electron	E137 [46], E141 [47], E774 [32] etc.
Neutrino trident	$\nu N \rightarrow \nu N \mu^+ \mu^-$	di-muon final state	LBNE [48], CCFR [49], DUNE [50]
ATLAS and CMS	$(i) pp \rightarrow Z' \rightarrow \mu^+ \mu^-$ $(ii) pp \rightarrow h, \phi \rightarrow Z^* Z',$ $Z^* Z' \rightarrow 4\ell$	(i) oppositely charged muons (ii) 4ℓ final state	(i) [51] (ii) [52, 53]
BaBar, Belle	$e^+ e^- \rightarrow \gamma_{\text{ISR}} Z'$ $, Z' \rightarrow \ell^+ \ell^- (\ell = e, \mu)$	lepton charged tracks with γ	BaBar [16, 31] Belle [30]
KLOE	$e^+ e^- \rightarrow \gamma_{\text{ISR}} Z',$ $Z' \rightarrow \mu^+ \mu^-, \pi^+ \pi^-$	charged tracks with γ	KLOE [54]

TABLE II: Summary of the existing laboratory-based constraints on light Z' . For further details see Ref. [16–21].

For the ease of readers, we denote the experimental constraints with the same notation for all $U(1)_X$ models shown in Fig.3-6. The bounds from $\text{E}\nu\text{ES}$ and $\text{CE}\nu\text{NS}$ from direct detection experiments (XENON1T) are shown by dark cyan and dark blue solid lines respectively. On the other hand bounds from Borexino and coherent scattering from CsI+Ar material are depicted by gray hatched region and dark green solid line respectively. The magenta solid line and the light blue hatched region in some figures signify the constraint from ν oscillation data [17] and fixed target experiments respectively. Finally, the 2σ upper limit on N_{eff} at

CMB (3.33) from Planck 2018 [5] is shown by the red dashed line. To display the variation of N_{eff} we also show two additional contours for $N_{\text{eff}} = 3.2$ and $N_{\text{eff}} = 3.5$ depicted by blue dashed lines. We now discuss each of the $U(1)_X$ models one by one throughout this section. Although two of them have already been discussed in the literature [7, 8], for completeness and comparative analysis, here we discuss all popular $U(1)_X$ models (see Table. I).

3.1. The Gauged $U(1)_{B-L}$ Symmetry

$B-L$ type of $U(1)_X$ model has been studied exhaustively in different contexts [20, 34, 35, 55]. In such gauge extensions, all three generation of leptons are charged with $U(1)_X$ charge $|\mathbb{X}_i| = 1$. Hence it lies to the first class of models which have tree level coupling of Z' with e^\pm as discussed in Sec.2. We show various constraints in $M_{Z'}$ vs. g_X plane in Fig.3(a). Since, in this model Z' can couple to both leptons and quarks it attracts strong constraints from fixed target experiments in the sub-GeV range of $M_{Z'}$ with $g_X \gtrsim 10^{-8}$ [32, 46, 47]. A summary of these bounds can be found in Refs. [56, 57]. On the other hand, neutrino scattering experiments like $\text{E}\nu\text{ES}$ and $\text{CE}\nu\text{NS}$ from XENON1T, XENONnT and LZ [20, 21, 43] place stringent constraint in the parameter space. Neutrino electron scattering from Borexino also excludes $g_X \gtrsim 10^{-5}$ for $M_{Z'} \sim 10$ MeV [18, 19, 44]. Other experiments like BaBar [31, 58] and KLOE [54] can place constraint at relatively larger couplings ($g_X \sim 10^{-4}$). In spite of these stringent constraints, there is significant parameter space, particularly for low mass and small couplings which remains unconstrained. The constraint coming from the upper limit on N_{eff} from Planck 2018 [5], shown by the red dashed line, can exclude a large portion of this parameter space as shown in Fig.3(a). It excludes $M_{Z'} \lesssim 5$ MeV at lower couplings ($g_X \sim 10^{-9}$) and $M_{Z'} \lesssim 20$ MeV at higher couplings ($g_X \sim 10^{-3}$). As discussed in Sec.2 with an increase in g_X the relevant collision terms increase leading to an enhancement in N_{eff} . And with an increase in $M_{Z'}$ the effect in N_{eff} decreases due to the suppressed energy density of Z' at ν_L decoupling. For this reason, we observe the contour for the upper limit on N_{eff} gradually shifts towards the higher $M_{Z'}$ with increase in g_X . This phenomenon can also be understood from the contour lines (blue dashed) with N_{eff} values of 3.5 and 3.2.

3.2. The Gauged $U(1)_{B-3L_i}$ Symmetry

So far we have considered only the flavour universal $U(1)_X$ symmetry where each generation of quarks and charged leptons carry the same charge under the $U(1)_X$ symmetry. However, there are several flavour dependent $U(1)_X$ symmetries known in the literature [15, 17–19, 59]. One of such flavour dependent $U(1)_X$ symmetry is the so called $U(1)_{B-3L_i}$ gauge symmetries [60]. In this scenario, the $U(1)_X$ charges of all generations of quarks are still the same as that we consider in $B-L$ symmetry, however only one generation of SM leptons carry the $U(1)_X$ charge. There are three types for such symmetries namely the

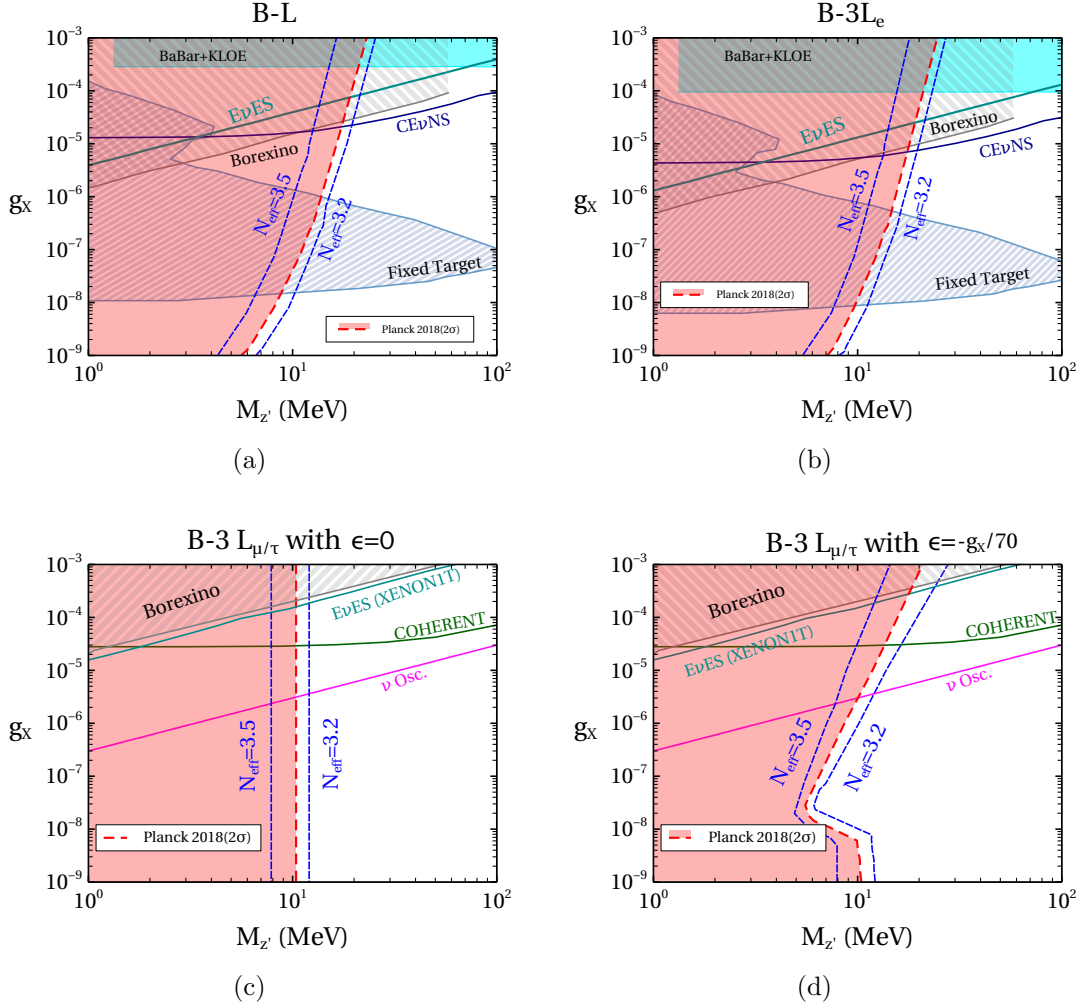


FIG. 3: Constraints from N_{eff} (Planck 2018) along with experimental bounds shown in the parameter space of light Z' realized in (a) $B - L$, (b) $B - 3L_e$, (c) $B - 3L_\mu$ with $\epsilon = 0$ and (d) $B - 3L_\mu$ with $\epsilon = -g_X/70$. The 2σ upper limit from Planck 2018 on N_{eff} is shown by the red dashed lines and the exclusion region is shown by the red shaded area.

$U(1)_{B-3L_e}$, $U(1)_{B-3L_\mu}$ and $U(1)_{B-3L_\tau}$ gauge symmetries corresponding to the first, second, and third generation of SM leptons respectively. The charges of the SM particles and new particles under these symmetries are given in Table I.

1. $B - 3L_e$ model:

In the $B - 3L_e$ model the light Z' couples to e^\pm apart from all 3 quark generations [59]. As the Z' has tree level coupling with e^\pm it will lie in the first class of models in deciding N_{eff} as discussed in Sec.2. Hence, the upper bound on N_{eff} arising from Planck 2018 also constrains this model, as depicted by the tilted red dashed line (similar to $B - L$) shown in Fig.3(b). However, in this case $U(1)_X$ charge of e^\pm , $|\mathbb{X}_1| = 3$ so the constraints will be

stronger than $B - L$ model. As the coupling of Z' with e^\pm is thrice ($\mathbb{X}_1 g_X$) than that of $B - L$ model, the relevant BSM processes also become larger compared to $B - L$, leading to larger N_{eff} for the same g_X and $M_{Z'}$. For this reason we notice the contour for the upper limit on N_{eff} shift towards the right (to higher $M_{Z'}$) as compared to $B - L$ shown in Fig.3(b). For the same reason the constraints like $\text{E}\nu\text{ES}$ and $\text{CE}\nu\text{NS}$ from Xenon1T [20], Borexino [18, 19, 44] become more stringent compared to $B - L$. Similar argument holds for BaBar [31, 58], KLOE [54] and fixed target experiments [16, 19, 32].

2. $B - 3L_{\mu/\tau}$ model:

In contrast to the $B - 3L_e$ model, in $B - 3L_\mu$ ($B - 3L_\tau$) model the light Z' couples to only second (third) generation of leptons with charge $|\mathbb{X}_2| = 3$ ($|\mathbb{X}_3| = 3$). As the Z' has no tree level coupling with e^\pm it will lie in the second class of models in deciding N_{eff} as discussed in Sec.2. If we do not assume any induced coupling between Z' and e^\pm , then the only BSM process to affect N_{eff} is the decay of Z' to ν_L sector with 100% branching ratio (BR). Thus all the Z' density eventually dilutes to ν_L sector independent of the coupling ($X_{2/3} g_X$) and hence we observe the bound from N_{eff} becomes a straight line in the M'_Z vs. g_X plane as shown in Fig.3(c). However, the situation changes drastically if we consider some induced coupling ⁷ $\epsilon = -g_X/70$ between Z' and e^\pm and the corresponding N_{eff} constraint is portrayed in Fig.3(d). The knee like pattern is due to the interplay between decay and scattering and is discussed in great detail in our earlier work [23]. In the presence of the induced coupling both the processes (i) scattering: $e^+e^- \rightarrow \nu\bar{\nu}$ mediated by Z' and (ii) decay $Z' \rightarrow e^+e^-/\nu\bar{\nu}$ are active in the higher coupling ($g_X \gtrsim 10^{-8}$) regime and the effect on N_{eff} becomes almost similar like $B - 3L_e$ in this regime. However, in the lower coupling regime $g_X \lesssim 10^{-8}$ the scatterings are suppressed ($\sim (g_X/70)^2$) than the decay ($\sim g_X^2$), and hence the BSM process becomes decay dominated [23]. Thus in this regime ($g_X \lesssim 10^{-8}$) the constraint from N_{eff} becomes independent of the coupling g_X . In the absence of tree level coupling with e^\pm , the experimental constraints in the parameter space are comparatively less stringent than those for $B - 3L_e$. The major constraints come from $\text{E}\nu\text{ES}$ from Xenon1T [20], Borexino [18, 19, 44] and COHERENT data [19]. Additionally, ν oscillation data also constrains the parameter space as given in Ref. [17].

3.3. The Gauged $U(1)_{L_i-L_j}$ Symmetry

So far we have been discussing about the $U(1)_X$ gauge symmetries under which at least some of the quarks were always charged. However, anomaly free models can be constructed by assigning $U(1)_X$ charges to even lepton sectors only. Such $U(1)_X$ models are $L_\mu -$

⁷ we pick this benchmark value to compare with the existing literature [39]

L_τ , $L_e - L_\mu$, and $L_e - L_\tau$ models. We start our discussion $L_\mu - L_\tau$ type models due to its wide discussion in the existing literature [7, 39].

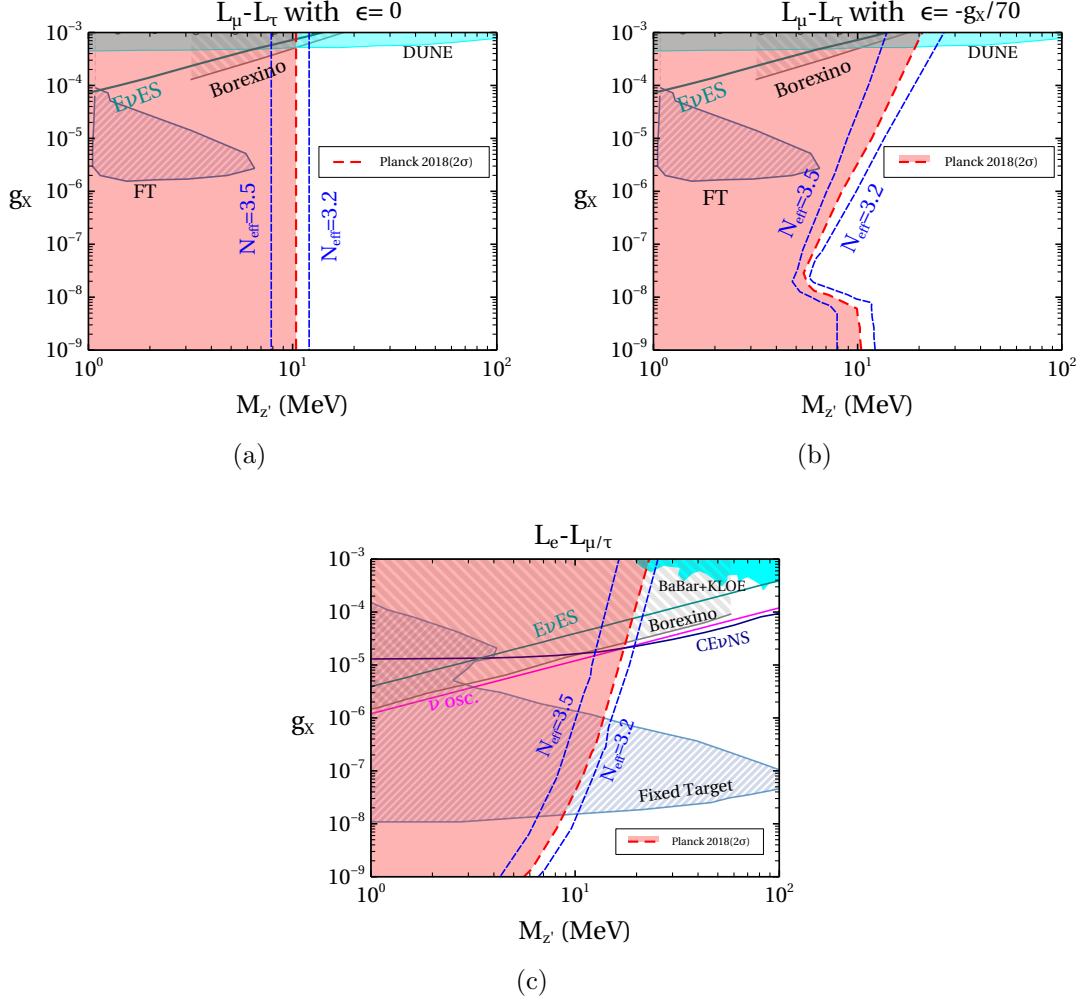


FIG. 4: Constraints from N_{eff} (Planck 2018) along with experimental bounds shown in the parameter space of light Z' realized in (a) $L_\mu - L_\tau$ with $\epsilon = 0$, (b) $L_\mu - L_\tau$ with $\epsilon = -g_X/70$ and (c) $L_e - L_\mu$. The 2σ upper limit from Planck 2018 on N_{eff} is shown by the red dashed lines and the exclusion region is shown by red shaded area.

1. $L_\mu - L_\tau$ model:

The N_{eff} upper limit contour in $L_\mu - L_\tau$ symmetry also exhibits similar dependence likewise in the $B - 3L_\mu$ model, due to the absence of tree level $Z'e^+e^-$ vertex. The constraints from N_{eff} with and without the induced couplings are shown in Fig.4(a) and Fig.4(b) respectively. In the sub-GeV range the other relevant constraints are E ν ES from Xenon1T [20], Borexino [18, 19, 44]. Fixed target (FT) experiment has very loose constraints due to the absence of both Z' quark coupling and Z' electron coupling [21].

2. $L_e - L_{\mu/\tau}$ model:

In $L_e - L_\mu$ (or $L_e - L_\tau$) model tree level $Z'e^+e^-$ vertex exists in contrast to $L_\mu - L_\tau$ type model and hence the constraint from N_{eff} is exactly same as $B - L$ model as depicted in Fig.4(c). For the same reason constraints from $\text{E}\nu\text{ES}$ from Xenon1T [21], Borexino [18, 19, 44], Babar [16, 31] and fixed target experiments [16, 32] are found to be stronger than $L_\mu - L_\tau$ model.

3.4. The Gauged $U(1)_{B_i-3L_j}$ Symmetry

There are also $U(1)_X$ symmetries where the symmetry is flavour dependent in both quarks as well as the lepton sector namely the $U(1)_{B_i-3L_j}$ gauge symmetries [15]. In this class, there are total nine such symmetries: $B_1 - 3L_j$, $B_2 - 3L_j$, $B_3 - 3L_j$ ($j \equiv e, \mu, \tau$), where B_1, B_2, B_3 correspond to the first, second and third generation of quarks respectively. For all nine cases, the charges of the ν_{R_i} can be fixed by the anomaly cancellation conditions. Among these nine symmetries, we discussed about $B_3 - 3L_j$ symmetry in our previous work [23]. In this work, we will shed light on the remaining six symmetries. The charge assignments of these symmetries are shown in Table I.

1. $B_i - 3L_e$ model:

Models like $B_1 - 3L_e$, $B_2 - 3L_e$, $B_3 - 3L_e$ fall in this category where Z' has tree level coupling with e^\pm and any one generation of quarks. Due to the presence of tree level $Z'e^+e^-$ vertex (with $|X_1| = 3$) the N_{eff} increases with increase in g_X for a fixed $M_{Z'}$. Hence the contour for the upper limit on N_{eff} exhibits a pattern similar to the $B - 3L_e$ model. The constraints are shown in Fig.5. For comparison, we also showcase bounds from $\text{E}\nu\text{ES}$ (from Xenon1T) [20], Borexino [44] which are similar to the case in $B - 3L_e$ model, since these bound rely only on the lepton coupling. Note that for $B_1 - 3L_e$ type of model with the tree level coupling of Z' to first generation quarks (and hence nucleons) may attract constraints from $\text{CE}\nu\text{NS}$, BaBar, and fixed target experiments. However such analysis has not been yet performed with these types of models in the existing literature and dedicated analysis is beyond the scope of this work. For $B_3 - 3L_e$ model due to the presence of $Z' - b$ coupling bound from $B_s - \bar{B}_s$ mixing is also applicable as shown in Ref. [23].

2. $B_i - 3L_{\mu/\tau}$ model:

In contrast to the previous case, in $B_i - 3L_{\mu/\tau}$ model Z' has no tree level coupling with e^\pm and thus the N_{eff} contour becomes independent of the coupling g_X as shown in Fig.6(a). However, in presence of induced coupling $\epsilon = -g_X/70$ the contour for N_{eff} follow pattern

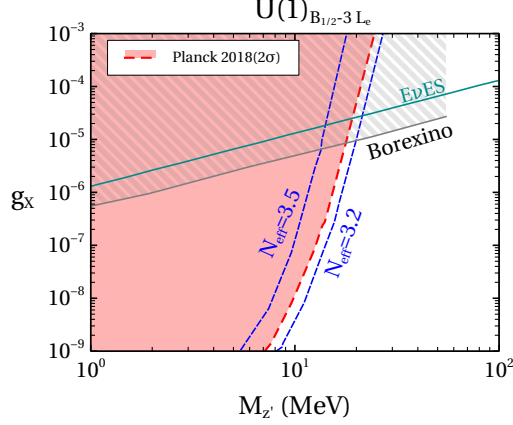


FIG. 5: Constraints from N_{eff} (Planck 2018) along with experimental bounds shown in the parameter space of light Z' realized in $B_{1/2} - 3L_e$. The 2σ upper limit from Planck 2018 on N_{eff} is shown by the red dashed lines and the exclusion region is shown by the red shaded area.

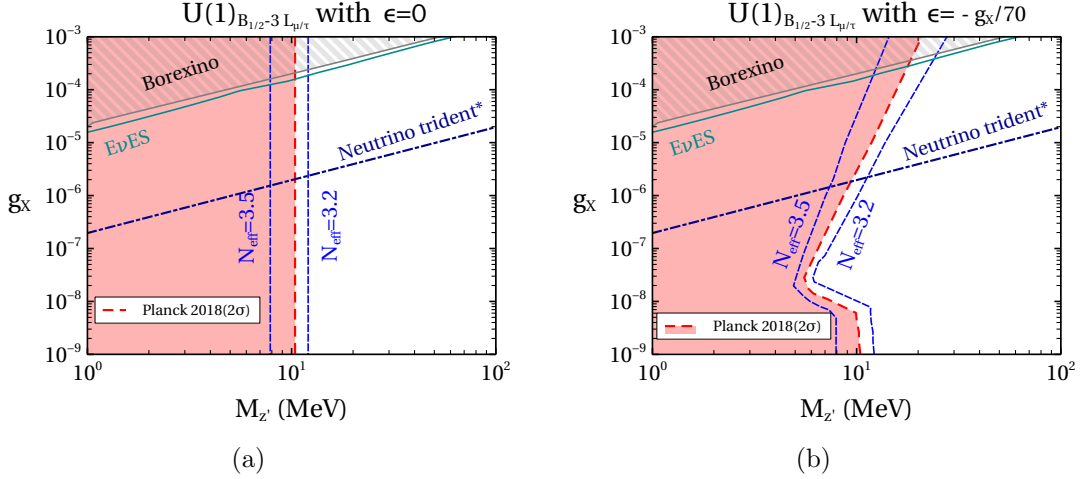


FIG. 6: Constraints from N_{eff} (Planck 2018) along with experimental bounds shown in the parameter space of light Z' realized in (a) $B_{1/2} - 3L_{\mu}$ with $\epsilon = 0$, (b) $B_{1/2} - 3L_{\mu}$ with $\epsilon = -g_X/70$. The 2σ upper limit from Planck 2018 on N_{eff} is shown by the red dashed lines and the exclusion region is shown by the red shaded area. The bound on $B_{1/2} - 3L_{\tau}$ parameter space will be similar to $B_{1/2} - 3L_{\mu}$ model except neutrino trident bound which is applicable to $B_1 - 3L_{\mu}$ type model only.

similar to $B - 3L_{\mu/\tau}$ as shown in Fig. 6(b). The knee like pattern of the contour for the upper bound on N_{eff} is due to the interplay between scattering and decay as already discussed earlier. Similar to the earlier case $B_i - 3L_{\mu/\tau}$ attracts constraints like $E\nu\text{ES}$ from Xenon1T [20], Borexino [19, 44] which are similar to the case in $B - 3L_{\mu}$ model. Here also we do not portray the bounds that may come from nuclear interactions. Additionally, $B_i - 3L_{\mu}$ type of model attracts strong constrain from neutrino trident experiment [15].

Thus the precise measurement of N_{eff} by Planck 2018 data [5] provides a unique oppor-

tunity to probe light Z' gauge bosons realized in various $U(1)_X$ models. In general, most of the terrestrial experiments looking for light Z' lose sensitivity in the sub-GeV mass range of Z' . Although the neutrino scattering experiments can constrain $M_{Z'} \ll \mathcal{O}(1)$ MeV, it can not probe very low couplings ($g_X \lesssim 10^{-6}$). On the other hand, the upper limit on N_{eff} by Planck 2018 can constrain $M_{Z'} \lesssim \mathcal{O}(1)$ MeV as well as very small couplings even upto $g_X \sim 10^{-9}$, as shown in this section. The value of N_{eff} relies on the ν_L decoupling and in the SM scenario it takes place around $T \sim \text{MeV}$ [6]. Hence N_{eff} is sensitive to BSM particles with sufficient energy at that temperature as in our case Z' with mass $M_{Z'} \sim 10$ MeV. For the same reason N_{eff} becomes insensitive to slightly heavier Z' with $M_{Z'} \gtrsim 30$ MeV, when the energy density becomes Boltzmann suppressed. Nevertheless the upper limit on N_{eff} can probe the parameter space which is beyond the reach of current ground based experiments. Astrophysical bounds like supernova may constrain very small couplings [61], however, such bounds largely depend on the modeling of the stellar objects [62]. Whereas the bound from N_{eff} is relatively more generic since here the only assumption is Z' to be a thermal bath which is the case for $g_X \gtrsim 10^{-9}$ [7].

4. CONCLUSIONS

The stringent limit on N_{eff} by Planck 2018 [5] can be used to constrain various BSM paradigms involving light ($\sim \mathcal{O}(\text{MeV})$) mediators. In this work, we show that the ν_L decoupling is significantly affected in the presence of light Z' particles interacting with ν (or, e^\pm) leading to an enhanced N_{eff} . This in turn leads to constraining the parameter space of light Z' in the mass ($M_{Z'}$) vs. coupling (g_X) plane using the Planck 2018 data. As the SM ν_L decoupling usually takes place at $T \sim 1$ MeV, N_{eff} upper limit puts strong constraint for $M_{Z'} \lesssim \text{few MeV}$. However, the ground based experiments looking for light BSM particles lose sensitivity in the sub-MeV range, and thus the constraint from N_{eff} can be useful in this regard. We consider several popular $U(1)_X$ models like $B - L$, $B - 3L_i$, $L_i - L_j$, $B_i - 3L_i$ and study the contribution in N_{eff} due to the light Z' realized in this model assuming Z' was initially in thermal bath. In our previous work [23], we showed the signature in N_{eff} due to the light Z' can be broadly classified into two categories depending on whether Z' has tree level coupling with e^\pm or not. We correctly identify the aforementioned Z' models and display the constraints from N_{eff} along with other existing constraints. For models with tree level $Z'e^+e^-$ coupling (e.g. $B - L$, $B - 3L_e$, $L_e - L_{\mu/\tau}$, $B_i - 3L_e$), the constraint from N_{eff} becomes stronger with an increase in g_X because of the enhancement in BSM processes with higher values of g_X . In the absence of tree level $Z'e^+e^-$ coupling N_{eff} is dominated by the decay, $Z' \rightarrow \nu\bar{\nu}$ and hence becomes insensitive to g_X . Thus we observe the N_{eff} constraints to be straight line in $M_{Z'}$ vs. g_X plane for such models (e.g. $B - 3L_{\mu/\tau}$, $L_\mu - L_\tau$, $B_i - 3L_{\mu/\tau}$). However, in the presence of induced $Z'e^+e^-$ couplings, the constraints modify due to the interplay of decay scattering as discussed in Sec.3. We observe that in a significant parame-

ter space, specifically for low Z' mass and small couplings, the constraint from N_{eff} is much more stringent than the experimental searches. In fact in many cases, the N_{eff} provides the only constraint on such parameter space. Thus looking at the footprints in N_{eff} at CMB can be an useful scheme to probe various light BSM particles having interactions with e^\pm or, ν_L .

Acknowledgments

SJ is funded by CSIR, Government of India, under the NET JRF fellowship scheme with Award file No. 09/080(1172)/2020-EMR-I. PG acknowledges the financial support through the APEX project at the Institute of Physics, Bhubaneswar. PG also acknowledges local hospitality at ICTS Bengaluru during the visit for the SATPP 2024.

-
- [1] S. Dodelson, *Modern Cosmology*. Academic Press, Amsterdam, 2003.
 - [2] G. Mangano, G. Miele, S. Pastor, T. Pinto, O. Pisanti, and P. D. Serpico, “Relic neutrino decoupling including flavor oscillations,” *Nucl. Phys. B* **729** (2005) 221–234, [arXiv:hep-ph/0506164](#).
 - [3] E. Grohs, G. M. Fuller, C. T. Kishimoto, M. W. Paris, and A. Vlasenko, “Neutrino energy transport in weak decoupling and big bang nucleosynthesis,” *Phys. Rev. D* **93** no. 8, (2016) 083522, [arXiv:1512.02205 \[astro-ph.CO\]](#).
 - [4] **Planck** Collaboration, P. A. R. Ade *et al.*, “Planck 2015 results. XIII. Cosmological parameters,” *Astron. Astrophys.* **594** (2016) A13, [arXiv:1502.01589 \[astro-ph.CO\]](#).
 - [5] **Planck** Collaboration, N. Aghanim *et al.*, “Planck 2018 results. VI. Cosmological parameters,” *Astron. Astrophys.* **641** (2020) A6, [arXiv:1807.06209 \[astro-ph.CO\]](#). [Erratum: *Astron. Astrophys.* 652, C4 (2021)].
 - [6] M. Escudero, “Neutrino decoupling beyond the Standard Model: CMB constraints on the Dark Matter mass with a fast and precise N_{eff} evaluation,” *JCAP* **02** (2019) 007, [arXiv:1812.05605 \[hep-ph\]](#).
 - [7] M. Escudero, D. Hooper, G. Krnjaic, and M. Pierre, “Cosmology with A Very Light $L_\mu - L_\tau$ Gauge Boson,” *JHEP* **03** (2019) 071, [arXiv:1901.02010 \[hep-ph\]](#).
 - [8] H. Esseili and G. D. Kribs, “Cosmological Implications of Gauged $U(1)_{B-L}$ on ΔN_{eff} in the CMB and BBN,” [arXiv:2308.07955 \[hep-ph\]](#).
 - [9] K. N. Abazajian and J. Heeck, “Observing Dirac neutrinos in the cosmic microwave background,” *Phys. Rev. D* **100** (2019) 075027, [arXiv:1908.03286 \[hep-ph\]](#).
 - [10] V. Poulin, T. L. Smith, T. Karwal, and M. Kamionkowski, “Early Dark Energy Can Resolve The Hubble Tension,” *Phys. Rev. Lett.* **122** no. 22, (2019) 221301, [arXiv:1811.04083 \[astro-ph.CO\]](#).

- [11] D. K. Ghosh, S. Jeusun, and D. Nanda, “Long-lived inert Higgs boson in a fast expanding universe and its imprint on the cosmic microwave background,” *Phys. Rev. D* **106** no. 11, (2022) 115001, [arXiv:2206.04940 \[hep-ph\]](#).
- [12] D. K. Ghosh, P. Ghosh, and S. Jeusun, “CMB signature of non-thermal Dark Matter produced from self-interacting dark sector,” *JCAP* **07** (2023) 012, [arXiv:2301.13754 \[hep-ph\]](#).
- [13] V. Poulin, T. L. Smith, D. Grin, T. Karwal, and M. Kamionkowski, “Cosmological implications of ultralight axionlike fields,” *Phys. Rev. D* **98** no. 8, (2018) 083525, [arXiv:1806.10608 \[astro-ph.CO\]](#).
- [14] T. Bringmann, F. Kahlhoefer, K. Schmidt-Hoberg, and P. Walia, “Converting nonrelativistic dark matter to radiation,” *Phys. Rev. D* **98** no. 2, (2018) 023543, [arXiv:1803.03644 \[astro-ph.CO\]](#).
- [15] C. Bonilla, T. Modak, R. Srivastava, and J. W. F. Valle, “ $U(1)_{B_3-3L_\mu}$ gauge symmetry as a simple description of $b \rightarrow s$ anomalies,” *Phys. Rev. D* **98** no. 9, (2018) 095002, [arXiv:1705.00915 \[hep-ph\]](#).
- [16] M. Bauer, P. Foldenauer, and J. Jaeckel, “Hunting All the Hidden Photons,” *JHEP* **07** (2018) 094, [arXiv:1803.05466 \[hep-ph\]](#).
- [17] P. Coloma, M. C. Gonzalez-Garcia, and M. Maltoni, “Neutrino oscillation constraints on $U(1)$ ’ models: from non-standard interactions to long-range forces,” *JHEP* **01** (2021) 114, [arXiv:2009.14220 \[hep-ph\]](#). [Erratum: *JHEP* 11, 115 (2022)].
- [18] P. Coloma, P. Coloma, M. C. Gonzalez-Garcia, M. C. Gonzalez-Garcia, M. Maltoni, M. Maltoni, J. a. P. Pinheiro, J. a. P. Pinheiro, S. Urrea, and S. Urrea, “Constraining new physics with Borexino Phase-II spectral data,” *JHEP* **07** (2022) 138, [arXiv:2204.03011 \[hep-ph\]](#). [Erratum: *JHEP* 11, 138 (2022)].
- [19] M. Atzori Corona, M. Cadeddu, N. Cargioli, F. Dordei, C. Giunti, Y. F. Li, E. Picciau, C. A. Ternes, and Y. Y. Zhang, “Probing light mediators and $(g-2)_\mu$ through detection of coherent elastic neutrino nucleus scattering at COHERENT,” *JHEP* **05** (2022) 109, [arXiv:2202.11002 \[hep-ph\]](#).
- [20] A. Majumdar, D. K. Papoulias, and R. Srivastava, “Dark matter detectors as a novel probe for light new physics,” *Phys. Rev. D* **106** no. 1, (2022) 013001, [arXiv:2112.03309 \[hep-ph\]](#).
- [21] V. De Romeri, D. K. Papoulias, and C. A. Ternes, “Light vector mediators at direct detection experiments,” [arXiv:2402.05506 \[hep-ph\]](#).
- [22] K. Chakraborty, A. Das, S. Goswami, and S. Roy, “Constraining general $U(1)$ interactions from neutrino-electron scattering measurements at DUNE near detector,” *JHEP* **04** (2022) 008, [arXiv:2111.08767 \[hep-ph\]](#).
- [23] D. K. Ghosh, P. Ghosh, S. Jeusun, and R. Srivastava, “Hubble Tension and Cosmological Imprints of $U(1)_X$ Gauge Symmetry: $U(1)_{B_3-3L_i}$ as a case study,” [arXiv:2312.16304](#)

- [hep-ph].
- [24] **CMS** Collaboration, V. Khachatryan *et al.*, “Search for narrow resonances in dilepton mass spectra in proton-proton collisions at $\sqrt{s} = 13$ TeV and combination with 8 TeV data,” *Phys. Lett. B* **768** (2017) 57–80, [arXiv:1609.05391 \[hep-ex\]](#).
 - [25] **ATLAS** Collaboration, G. Aad *et al.*, “Search for high-mass dilepton resonances using 139 fb⁻¹ of pp collision data collected at $\sqrt{s} = 13$ TeV with the ATLAS detector,” *Phys. Lett. B* **796** (2019) 68–87, [arXiv:1903.06248 \[hep-ex\]](#).
 - [26] A. Das, S. Oda, N. Okada, and D.-s. Takahashi, “Classically conformal U(1)’ extended standard model, electroweak vacuum stability, and LHC Run-2 bounds,” *Phys. Rev. D* **93** no. 11, (2016) 115038, [arXiv:1605.01157 \[hep-ph\]](#).
 - [27] E. Accomando, L. Delle Rose, S. Moretti, E. Olaiya, and C. H. Shepherd-Themistocleous, “Extra Higgs boson and Z' as portals to signatures of heavy neutrinos at the LHC,” *JHEP* **02** (2018) 109, [arXiv:1708.03650 \[hep-ph\]](#).
 - [28] R. Essig, P. Schuster, and N. Toro, “Probing Dark Forces and Light Hidden Sectors at Low-Energy $e+e-$ Colliders,” *Phys. Rev. D* **80** (2009) 015003, [arXiv:0903.3941 \[hep-ph\]](#).
 - [29] **LHCb** Collaboration, R. Aaij *et al.*, “Search for Dark Photons Produced in 13 TeV pp Collisions,” *Phys. Rev. Lett.* **120** no. 6, (2018) 061801, [arXiv:1710.02867 \[hep-ex\]](#).
 - [30] G. Inguglia, “Belle II studies of missing energy decays and searches for dark photon production,” *PoS DIS2016* (2016) 263, [arXiv:1607.02089 \[hep-ex\]](#).
 - [31] **BaBar** Collaboration, J. P. Lees *et al.*, “Search for a Dark Photon in e^+e^- Collisions at BaBar,” *Phys. Rev. Lett.* **113** no. 20, (2014) 201801, [arXiv:1406.2980 \[hep-ex\]](#).
 - [32] A. Bross, M. Crisler, S. H. Pordes, J. Volk, S. Errede, and J. Wrbanek, “A Search for Shortlived Particles Produced in an Electron Beam Dump,” *Phys. Rev. Lett.* **67** (1991) 2942–2945.
 - [33] **COHERENT** Collaboration, D. Akimov *et al.*, “Measurement of the Coherent Elastic Neutrino-Nucleus Scattering Cross Section on CsI by COHERENT,” *Phys. Rev. Lett.* **129** no. 8, (2022) 081801, [arXiv:2110.07730 \[hep-ex\]](#).
 - [34] E. Ma and R. Srivastava, “Dirac or inverse seesaw neutrino masses with $B - L$ gauge symmetry and S_3 flavor symmetry,” *Phys. Lett. B* **741** (2015) 217–222, [arXiv:1411.5042 \[hep-ph\]](#).
 - [35] E. Ma, N. Pollard, R. Srivastava, and M. Zakeri, “Gauge $B - L$ Model with Residual Z_3 Symmetry,” *Phys. Lett. B* **750** (2015) 135–138, [arXiv:1507.03943 \[hep-ph\]](#).
 - [36] R. N. Mohapatra and G. Senjanovic, “Neutrino Mass and Spontaneous Parity Nonconservation,” *Phys. Rev. Lett.* **44** (1980) 912.
 - [37] J. Schechter and J. W. F. Valle, “Neutrino Masses in SU(2) x U(1) Theories,” *Phys. Rev. D* **22** (1980) 2227.
 - [38] D. W. P. d. Amaral, D. G. Cerdeno, P. Foldenauer, and E. Reid, “Solar neutrino probes of the muon anomalous magnetic moment in the gauged U(1) _{$L_\mu - L_\tau$} ,” *JHEP* **12** (2020) 155,

- [arXiv:2006.11225 \[hep-ph\]](#).
- [39] H. Banerjee, B. Dutta, and S. Roy, “Probing $L\mu$ - $L\tau$ models with $CE\nu$ NS: A new look at the combined COHERENT CsI and Ar data,” *Phys. Rev. D* **104** no. 1, (2021) 015015, [arXiv:2103.10196 \[hep-ph\]](#).
 - [40] D. F. G. Fiorillo, G. G. Raffelt, and E. Vitagliano, “Strong Supernova 1987A Constraints on Bosons Decaying to Neutrinos,” *Phys. Rev. Lett.* **131** no. 2, (2023) 021001, [arXiv:2209.11773 \[hep-ph\]](#).
 - [41] D. F. G. Fiorillo, G. G. Raffelt, and E. Vitagliano, “Large Neutrino Secret Interactions Have a Small Impact on Supernovae,” *Phys. Rev. Lett.* **132** no. 2, (2024) 021002, [arXiv:2307.15115 \[hep-ph\]](#).
 - [42] H. T. Janka, “Neutrino Emission from Supernovae,” [arXiv:1702.08713 \[astro-ph.HE\]](#).
 - [43] S. K. A., A. Majumdar, D. K. Papoulias, H. Prajapati, and R. Srivastava, “Implications of first LZ and XENONnT results: A comparative study of neutrino properties and light mediators,” *Phys. Lett. B* **839** (2023) 137742, [arXiv:2208.06415 \[hep-ph\]](#).
 - [44] A. N. Khan, W. Rodejohann, and X.-J. Xu, “Borexino and general neutrino interactions,” *Phys. Rev. D* **101** no. 5, (2020) 055047, [arXiv:1906.12102 \[hep-ph\]](#).
 - [45] M. Cadeddu, N. Cargioli, F. Dordei, C. Giunti, Y. F. Li, E. Picciau, and Y. Y. Zhang, “Constraints on light vector mediators through coherent elastic neutrino nucleus scattering data from COHERENT,” *JHEP* **01** (2021) 116, [arXiv:2008.05022 \[hep-ph\]](#).
 - [46] J. D. Bjorken, S. Ecklund, W. R. Nelson, A. Abashian, C. Church, B. Lu, L. W. Mo, T. A. Nunamaker, and P. Rassmann, “Search for Neutral Metastable Penetrating Particles Produced in the SLAC Beam Dump,” *Phys. Rev. D* **38** (1988) 3375.
 - [47] E. M. Riordan *et al.*, “A Search for Short Lived Axions in an Electron Beam Dump Experiment,” *Phys. Rev. Lett.* **59** (1987) 755.
 - [48] W. Altmannshofer, S. Gori, M. Pospelov, and I. Yavin, “Neutrino Trident Production: A Powerful Probe of New Physics with Neutrino Beams,” *Phys. Rev. Lett.* **113** (2014) 091801, [arXiv:1406.2332 \[hep-ph\]](#).
 - [49] **CCFR** Collaboration, S. R. Mishra *et al.*, “Neutrino Tridents and W Z Interference,” *Phys. Rev. Lett.* **66** (1991) 3117–3120.
 - [50] W. Altmannshofer, S. Gori, J. Martín-Albo, A. Sousa, and M. Wallbank, “Neutrino Tridents at DUNE,” *Phys. Rev. D* **100** no. 11, (2019) 115029, [arXiv:1902.06765 \[hep-ph\]](#).
 - [51] **CMS** Collaboration, A. M. Sirunyan *et al.*, “Search for a Narrow Resonance Lighter than 200 GeV Decaying to a Pair of Muons in Proton-Proton Collisions at $\sqrt{s} = \text{TeV}$,” *Phys. Rev. Lett.* **124** no. 13, (2020) 131802, [arXiv:1912.04776 \[hep-ex\]](#).
 - [52] **ATLAS** Collaboration, G. Aad *et al.*, “Measurements of Four-Lepton Production at the Z Resonance in pp Collisions at $\sqrt{s} = 7$ and 8 TeV with ATLAS,” *Phys. Rev. Lett.* **112** no. 23, (2014) 231806, [arXiv:1403.5657 \[hep-ex\]](#).
 - [53] **CMS** Collaboration, S. Chatrchyan *et al.*, “Observation of Z Decays to Four Leptons with

- the CMS Detector at the LHC,” *JHEP* **12** (2012) 034, [arXiv:1210.3844 \[hep-ex\]](#).
- [54] **KLOE-2** Collaboration, A. Anastasi *et al.*, “Combined limit on the production of a light gauge boson decaying into $\mu^+\mu^-$ and $\pi^+\pi^-$,” *Phys. Lett. B* **784** (2018) 336–341, [arXiv:1807.02691 \[hep-ex\]](#).
- [55] S. Mandal, H. Prajapati, and R. Srivastava, “ $B - L$ model in light of the CDF II result,” [arXiv:2301.01522 \[hep-ph\]](#).
- [56] J. D. Bjorken, R. Essig, P. Schuster, and N. Toro, “New Fixed-Target Experiments to Search for Dark Gauge Forces,” *Phys. Rev. D* **80** (2009) 075018, [arXiv:0906.0580 \[hep-ph\]](#).
- [57] R. Harnik, J. Kopp, and P. A. N. Machado, “Exploring ν Signals in Dark Matter Detectors,” *JCAP* **07** (2012) 026, [arXiv:1202.6073 \[hep-ph\]](#).
- [58] **BaBar** Collaboration, J. P. Lees *et al.*, “Search for Invisible Decays of a Dark Photon Produced in e^+e^- Collisions at BaBar,” *Phys. Rev. Lett.* **119** no. 13, (2017) 131804, [arXiv:1702.03327 \[hep-ex\]](#).
- [59] V. De Romeri, A. Majumdar, D. K. Papoulias, and R. Srivastava, “XENONnT and LUX-ZEPLIN constraints on DSNB-boosted dark matter,” *JCAP* **03** (2024) 028, [arXiv:2309.04117 \[hep-ph\]](#).
- [60] E. Ma, “Gauged B - 3L(τ) and radiative neutrino masses,” *Phys. Lett. B* **433** (1998) 74–81, [arXiv:hep-ph/9709474](#).
- [61] K. Akita, S. H. Im, and M. Masud, “Probing non-standard neutrino interactions with a light boson from next galactic and diffuse supernova neutrinos,” *JHEP* **12** (2022) 050, [arXiv:2206.06852 \[hep-ph\]](#).
- [62] N. Bar, K. Blum, and G. D’Amico, “Is there a supernova bound on axions?,” *Phys. Rev. D* **101** no. 12, (2020) 123025, [arXiv:1907.05020 \[hep-ph\]](#).